Exploring polymorphism and stoichiometric diversity in naproxen/proline cocrystals

Tumanova, Natalia; Tumanov, Nikolay; Fischer, Franziska; Morelle, Fabrice; Ban, Voraksmy; Robeyns, Koen; Filinchuk, Yaroslav; Wouters, Johan; Emmerling, Franziska; Leyssens, Tom

Published in:
CrystEngComm

DOI:
10.1039/C8CE01338A

Publication date:
2018

Document Version
Peer reviewed version

Journal Name

ARTICLE

Exploring Polymorphism and Stoichiometric Diversity in Naproxen/Proline Cocrystals

Received 00th January 20xx,
Accepted 00th January 20xx

DOI: 10.1039/x0xx00000x

www.rsc.org/

Natalia Tumanova[a], Nikolay Tumanov[b], Franziska Fischer[c], Fabrice Morelle[a], Voraksmy Ban[d], Koen Robeyns[a], Yaroslav Filinchuk[a], Johan Wouters[b], Franziska Emmerling[c] and Tom Leyssens*[a]

We present naproxen/proline cocrystals discovered when combining enantiopure and racemic naproxen and proline. Using liquid-assisted grinding as a main method to explore the variaty of crystal forms in this system, we found 17 cocrystals, the structures of only four of them were previously known. Naproxen/proline system exhibited multiple polymorphs of 1:1 stoichiometry, as well as more rare cocrystals with 1:2 and 2:3 stoichiometries, two cocrystal hydrates and one cocrystal solvate. *In situ* ball-milling, used to monitor liquid-assisted grinding reactions, revealed that solvent dictates the reaction intermediates, even if the final reaction product stays the same. Synchrotron X-ray diffraction data collected *in situ* upon heating allowed us to monitor directly phase changes upon heating and gave access to pure diffraction patterns of several cocrystals thus enabling their structure determination from powder X-ray diffraction data; this method also confirmed the formation of a conglomerate in the RS-naproxen/DL-proline system. Proline in cocrystals kept its ability to form charge-assisted head-to-tail N–H…O hydrogen bonds, typical of pure crystalline amino acids, thus increasing the percentage of strong charge-assisted interactions in the structure and consequently providing some of the cocrystals with higher melting points as compared to pure naproxen. The majority of drugs are chiral, and hence, these data are of importance to pharmacetical industry as they provide insight into challenges of chiral cocrystallization.

Introduction

Multicomponent crystalline systems had been known long before the term "cocrystal" gained its popularity.[1,2] The field of cocrystallization and the concept of crystal engineering has especially flourished in the last decades. Engineering cocrystals has become a widespread solution to various structure-property related problems, *e.g.*, improving therapeutic performance of drugs in pharmaceutical industry[3–5] or tuning properties of thermo- and photochromic materials, molecular semiconductors and optical materials.[6–10]

Chiral cocrystals are of special importance in pharmaceutical industry as a substantial part of drugs are chiral.[11] Knowing how the enantiomeric or racemic forms of the same drug would respond to cocrystallization with chiral and/or non-chiral coformers, *i.e.*, the differences in both the structure and properties of those cocrystals, their ability to cocrystallization, production related issues, is essential in developing robust and effective crystallization processes. There have been a number of works in this area. For instance, caffeine and theophylline were found to respond differently to cocrystallization with DL- and D-tartaric acid.[12,13] Enantiospecific behavior, when only one of the enantiomers was found to form a cocrystal with a certain chiral coformer, was reported for various systems, *e.g.*, the stanolone/tartaric acid[14], cyclohexandiol/tartaric acid[15], levetiracetam/mandelic acid and levetiracetam/tartaric acid[16], naproxen/tyrosine[17] systems. This property of chiral cocrystals was used to develop alternative chiral resolution techniques based on cocrystallization.[18–24]

Amino acids, except glycine, are chiral. Their use in pharmaceutical industry as potential coformers can be advantageous as they are natural to the body and thus present significantly lower risks in comparison with other coformers. Amino acids are zwitterionic in the crystalline state and tend to form head-to-tail charge-assisted hydrogen bonded chains[25–27] that are also observed in cocrystals[17,28]; this structural feature of amino acids may help to improve the API's properties, for instance by increasing stability, as the percentage of strong interactions in the structure grows.[29]

Proline is special as, unlike other amino acids, its amino group is found within the pyrrolidine ring. It showed a good ability to cocrystallize with various compounds for multiple applications, *i.e.*, to alter physicochemical properties of drugs[30–35], for chiral resolution[36–38], to develop an amino acid derived

[a] IMCN Institute of Condensed Matter and Nanosciences, Université catholique de Louvain, Place Louis Pasteur 1, 1348 Louvain-la-Neuve, Belgium. E-mail: tom.leyssens@uclouvain.be
[b] Chemistry Department, University of Namur, Rue de Bruxelles 61, 5000 Namur, Belgium.
[c] BAM Federal Institute for Materials Research and Testing, Richard-Willstätter-Strasse 11, 12489 Berlin, Germany.
[d] MS-Group, Swiss Light Source, Paul Scherrer Institute, 5232 Villigen PSI, Switzerland.

†Electronic Supplementary Information (ESI) available: Experimental details on structure determination, along with additional experimental details of sample preparation and sample analysis, including DSC and PXRD data. See DOI: 10.1039/x0xx00000x

semiconductor[39], etc. Proline has also been used for ionic cocrystal formation to investigate the possibilities of chiral resolution in the solid state[40].

In our recent work, we combined enantiopure and racemic forms of flurbiprofen and proline and, with the help of various state-of-the-art characterization methods, identified 17 cocrystals.[41] In this work, we chose another model compound, naproxen, to study cocrystallization of chiral coformers. Naproxen is a nonsteroidal anti-inflammatory drug poorly soluble in water; several cocrystals of naproxen have already been developed with the purpose of modifying its properties.[42] Its cocrystallization with amino acids may suggest an alternative way to improve its therapeutic performance. Naproxen has already shown its ability to cocrystallize with amino acids, such as alanine, tryptophan, tyrosine[17], arginine[43]. In addition, several cocrystals of naproxen (**nprx**) and proline (**pro**) have been previously reported.[28] In this work, applying a combination of modern characterization methods, including synchrotron X-ray diffraction upon various conditions, we discovered multiple previously unknown **nprx**/**pro** cocrystal phases. The **nprx**/**pro** system, with its 17 cocrystals (including two cocrystal hydrates and one cocrystal solvate) and one conglomerate, is another fascinating example of complexity that can be reached in a chiral system when using **pro** as a coformer.

Experimental

Experimental procedures are described below, except the procedure for the production of single crystals and structure determination from single-crystal and powder X-ray diffraction data which are given in ESI.

Materials

All the compounds for this work were purchased from Sigma-Aldrich and used without further purification. The reference diffraction patterns of the initial compounds were simulated using the Mercury software[44] from the corresponding structures found in the Cambridge Structural Database: **S-nprx** (CCDC COYRUD[45], COYRUD11[46], and COYRUD12[47]), **RS-nprx** (CCDC PAPTUX[48] and PAPTUX01[49]), **L-pro** (CCDC PROLIN[50], PROLIN02[41], and PROLIN03[41]), **L-pro monohydrate** (CCDC RUWGEV[51]), **DL-pro** (CCDC QANRUT[52] and QANRUT01[53]), and **DL-pro monohydrate** (CCDC DLPROM01[54]).

Laboratory liquid-assisted grinding (LAG) and laboratory powder X-ray diffraction analysis.

Liquid-assisted grinding in the presence of five different solvents, methanol (MeOH), ethanol (EtOH), isopropanol (ISPN), acetonitrile (ACN), and water was performed for five combinations of enantiopure and racemic **nprx** and **pro**: **S-nprx/L-pro**, **S-nprx/D-pro**, **S-nprx/DL-pro**, **RS-nprx/L-pro**, and **RS-nprx/DL-pro**. The compounds were ground in 1:1, 1:2, 2:3, and 2:1 ratios. To prepare each sample, 50-100 mg of total powder were placed into 2 mL Eppendorf tube, 2-10 µL of solvent were added, along with 5-6 stainless steel 2 mm balls to ensure grinding; the Eppendorf tubes were placed into a Retsch MM400 mixer mill for 60 min at a frequency of 30 Hz.

Resultant powders were analyzed by powder X-ray diffraction (PXRD), Cu*K*α radiation, using a Siemens D5000 diffractometer (2θ was scanned from 2 to 50° with a step of 0.02°) or a X'pert PRO PANalytical diffractometer (2θ scanned from 4 to 50° with a step of 0.017°). Collected diffraction patterns were analyzed by comparison with those of initial pure compounds and other known cocrystal phases in order to identify whether or not anything new formed.

Some samples were chosen for further analysis by other methods. All LAG experiments, their outcome, and characterization methods are summarized in Tables S4.1, S5.1, S6.1, S7.1, S8.1, and S9.1.

In situ synchrotron variable temperature X-ray diffraction data collection.

Selected powders obtained by liquid-assisted grinding were packed into 0.5 mm glass capillaries and measured upon heating at a rate of 2 °C/min. All powder diffraction data, except *in situ* experiment for the **1:1 RS-nprx/L-pro/H_2O** (sample *17* in Table S7.1) and **1:1 RS-nprx/DL-pro/H_2O** (sample *17* in Table S8.1), were collected using synchrotron radiation source: MS-X04SA beam line at the Swiss Light Source (SLS) (PSI, Switzerland) equipped with a 1D microstrip detector MYTHEN II. The measurements were performed at λ = 0.77663, 0.62173, 0.708 Å with a step of 0.0036°. The wavelength was calibrated using a standard NIST 640d Si sample. Selected diffraction patterns were used for structure determination from X-ray powder data. The **1:1 RS-nprx/L-pro/H_2O** (sample *17* in Table S7.1) and **1:1 RS-nprx/DL-pro/H_2O** (sample *17* in Table S8.1) were measured at the Swiss-Norwegian beamline BM1A at the European Synchrotron Radiation Facility (ESRF) (Grenoble, France), using a PILATUS 2M hybrid pixel detector at a wavelength of 0.78487 Å.

In situ ball-milling synchrotron X-ray diffraction data collection.

In situ ball-milling X-ray diffraction experiments were performed at the µSpot beamline (BESSY II, Helmholtz Centre Berlin for Materials and Energy, Germany) using a Pulverisette 23 (Fritsch, Germany) ball mill and Perspex jars; the frequency was 50 Hz. Compounds were mixed and the solvent and 3 stainless 5 mm steel balls were added right before the experiment. Details for each experiment (duration of milling, amount of solvent, amounts of initial compounds) are summarized in Table S3.1 A beam diameter of 100 µm at a photon flux of 1×10^9 s $^{-1}$ at a ring current of 100 mA was used. The experiments were performed at a wavelength of 1.000 Å using a double crystal monochromator Si (111). The spot size on the sample was 200 µm. Scattered intensities were collected with a two-dimensional X-ray detector (MarMosaic, CCD 3072 × 3072 pixels, pixel size 73 µm)[55]. Measurements were carried out every 30 s with a delay time of 3 or 4 s between two measurements. The occasionally observed doubling of reflections is caused by diffraction of two

different areas in the reaction jar, due to differences in the distance between the detector and the sample. Obtained two-dimensional diffraction images were integrated (2θ vs intensity) using the program Fit2D[56]. Diffraction patterns were background corrected and plotted as 2D film representation using the Powder3D program[57].

Differential scanning calorimetry (DSC) and thermogravimetric analysis (TGA).

DSC curves were measured using a DSC 821 Mettler Toledo instrument. Prior to measurements, the instrument was calibrated using indium. Standard 40 µL aluminum crucibles were used. The heating rate was 2 °C/min over the range from 25 to 200-250 °C. All experiments were carried out under nitrogen atmosphere (a flow rate of 50 ml/min). DSC curves of the selected samples are given in ESI.

DSC data were used to select multiphase samples and to determine melting points when possible. Samples with complicated DSC curve shapes were further analyzed *in situ* using variable-temperature synchrotron radiation in order to identify and directly monitor phase changes upon heating. It should be noted that direct matching of the DSC and *in situ* synchrotron PXRD data may not be always reliable due to different experimental setups; however, *in situ* synchrotron PXRD data provide a more profound view and might help in interpretation of the DSC data.

TGA curve was measured in order to determine the number of water molecules in the asymmetric unit of the **1:1 S/DL/H_2O** cocrystal hydrate (sample *17* in Table S9.1) needed to solve the structure of this phase from PXRD. The measurement was performed in the temperature range from 25 to 400 °C and at a heating rate of 5 °C/min using a Mettler Toledo TGA/DSC 3+ instrument; the obtained TGA curve is given in Fig. S9.3.6.

Results and Discussion

We studied five combinations of enantiopure and racemic naproxen and proline: **S-nprx/L-pro** (=**R-nprx/D-pro**), **S-nprx/D-pro** (=**R-nprx/L-pro**), **S-nprx/DL-pro** (=**R-nprx/DL-pro**), **RS-nprx/L-pro** (=**RS-nprx/D-pro**), and **RS-nprx/DL-pro**. The main approach to explore cocrystal phases was liquid-assisted grinding (LAG); solution cocrystallization was used only to produce single crystals. The advantages of LAG were outlined in our previous work[41], where this method proved highly efficient. LAG was performed in the presence of the following five solvents and varying the ratio of the initial compounds: methanol (MeOH), ethanol (EtOH), isopropanol (ISPN), acetonitrile (ACN), and water. The solvents were chosen so that at least one of the initial compounds will be well soluble: **nprx** is relatively well soluble in all the solvents except water, whereas **pro** exhibits decent solubility only in MeOH, EtOH, and water. Powders obtained after LAG reactions were subjected first to simple laboratory PXRD analysis in order to identify known phases, then DSC analysis was performed for selected samples in order to check for both the purity of the samples and any occurring phase transformations, as well as to determine the melting points if possible. The samples that exhibited complicated DSC curves with multiple peaks were further subjected to variable-temperature *in situ* synchrotron X-ray diffraction analysis to gain a direct insight into phase changes. The structures of those cocrystal phases for which we failed to grow sufficiently big single-crystals for single-crystal X-ray diffraction analysis were solved from powder X-ray diffraction data collected using synchrotron radiation. Scheme 1 gives an overview of the results. As all the combinations, except **S/D**, resulted in multiple cocrystal phases, we decided to perform *in situ* ball-milling experiments monitored by synchrotron radiation in order to get a deeper insight into mechanochemical reactions. Each combination is discussed below in detail. The structures of obtained cocrystals are discussed in the Structural Analysis section.

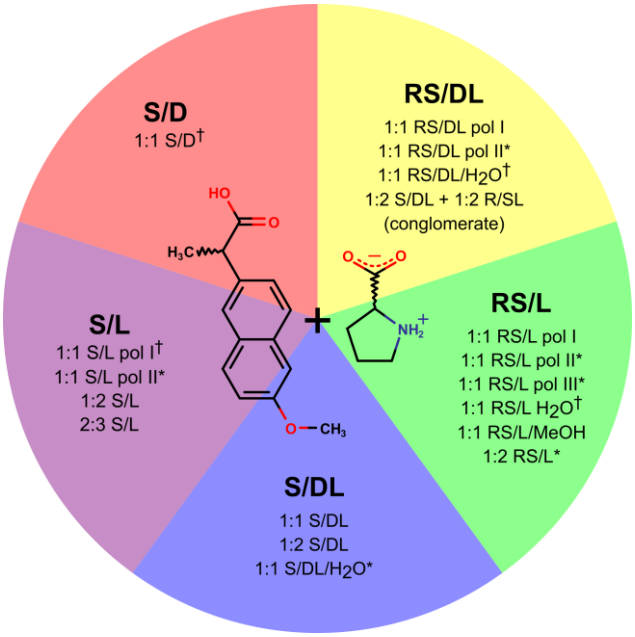

Scheme 1. A schematic summary of all the found cocrystals for the five **nprx/pro** combinations. Already known cocrystal phases and the phases whose structures were determined from powder X-ray diffraction data are marked as '†' and '*', respectively; the structures of all the other left phases were determined from single-crystal X-ray diffraction data.

S-naproxen/L-proline (S/L)

S/L system yielded the richest variety of cocrystals, including cocrystals with a different stoichiometry. All the cocrystals whose structures were determined can be found in Scheme 1. Preliminary laboratory LAG experiments with a series of solvents (MeOH, EtOH, ISPN, and ACN) did not allow us to draw any reliable conclusions about whether or not the reaction outcome is solvent-dependent: all the phases seemed to have chances to emerge. Table S4.1 summarizes the outcomes of the laboratory LAG experiments. From this table we see that, among the 1:1 forms, **1:1 S/L pol I** (CCDC REF FEVZUD[28]) seemed to emerge more often in MeOH- and EtOH-LAG reactions, whereas ACN- and ISPN-LAG resulted mainly in the **1:1 S/L pol II**. However, some samples contained both polymorphs in varied amounts. LAG reactions when **pro** was taken in an excess amount (1:2 and 2:3 **nprx** : **pro** ratios)

showed the formation of the **2:3 S/L** cocrystal, whereas the 2:1 **nprx** : **pro** ratio yielded mainly **1:1 S/L** polymorphs. The **1:2 S/L**

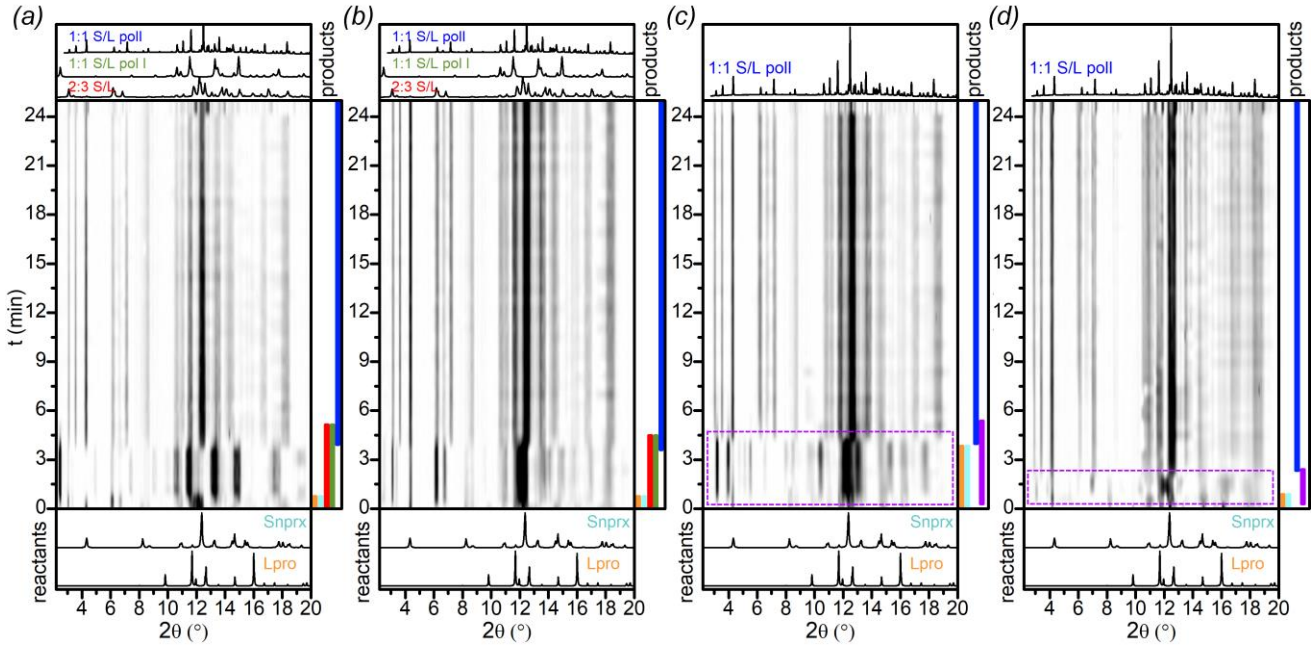

Figure. 1 *In situ* ball-milling X-ray diffraction patterns for the **S/L** system, λ = 1 Å, 1:1 ratio: (*a*) MeOH-, (*b*) EtOH-, (*c*) ISPN-, and (*d*) ACN-LAG. Colored bands on the right side of each image represent the presence of phases and are shown only for illustrative purpos; the area outlined by purple in (*c*) and (*d*) shows the presence of the **unknown phase I**

cocrystal that was crystallized from solution during our attempts to obtain single crystals was detected only in 1:2 water-LAG and 2:3 ISPN-LAG (see samples *12* and *18* in Table S4.1) and not in any other LAG reactions, even if the initial ratio of the components was 1:2 (see samples *2*, *6*, *10*, and *14* in Table S4.1). As can be seen from Table S4.1, most of the laboratory LAG experiments led to product mixtures, which means that the cocrystal phases kinetically compete with one another. We performed *in situ* ball-milling experiments in order to gain insight into the grinding process and directly monitor the phase changes in the course of the reaction. The results are presented in Figure 1.

All the *in situ* monitored LAG reactions finally led to the **1:1 S/L pol II** phase, but the pathway differed (samples *1-4* in Table S3.1). In MeOH- and EtOH-LAG, a mixture of the **1:1 S/L pol I** and **2:3 S/L** preceded the formation of the **1:1 S/L pol II** (Figures 1a, b; Fig. S3.1.1 and S3.1.2) and disappeared by the 6th minute of reaction, thus indicating that the former phases are more kinetically favored under these conditions, but not stable enough to withstand further grinding. In ISPN- and ACN-LAG (Figures 1c, d), we saw an unknown phase emerging in the beginning and then disappearing during the course of reaction (we called it **unknown phase I**), which thus was as well less stable, but kinetically faster than **1:1 S/L pol II** under those grinding conditions. Hence, *in situ* ball-milling experiments showed that varying the solvent affects the reaction pathway, by revealing the formation of different phases that precede the main **1:1 S/L pol II** phase depending on the solvent used – the result that was not apparent in the laboratory experiments.

In situ ball-milling reaction outcomes differed from those obtained by 1:1 laboratory LAG: in laboratory experiments (1:1 ratio) both **1:1 S/L pol I** and **1:1 S/L pol II** had chances to emerge, unlike the *in situ* ball-milled powders that contained only **pol II** as the final reaction product, no matter which solvent was used. This result can be explained by the fact that grinding reactions may be very sensitive to the ball-milling setup (the amount of powder, the diameter of balls, the volume of liquid added per total amount of powder, the jar's configuration and the material the jar is made of, etc.).

However, despite the difference, we can still make some parallels between the laboratory and *in situ* ball-milling data. For instance, the precedence of the **1:1 S/L pol I** to the emergence of the **1:1 S/L pol II** in MeOH-LAG (Figure 1a) indicates that these two polymorphs compete with each other, which explains why in some 1:1 laboratory grinding reactions we obtained one or another or both polymorphs at the same time, depending on the conditions.

DSC curves measured for selected samples (see Figs. S4.3.1-S4.3.5) had complex shapes with multiple peaks. This is why we decided to measure variable-temperature *in situ* synchrotron PXRD for those samples in order to monitor phase changes upon heating.

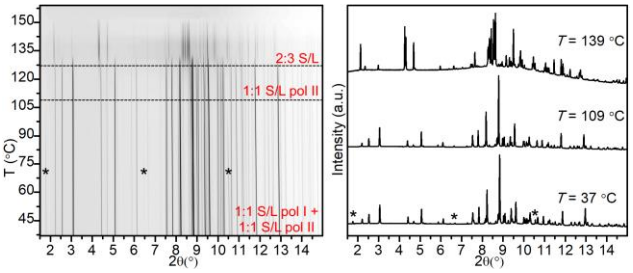

Figure 2. PXRD patterns measured in situ upon heating (from 37 to 159 °C, 2 °C/min) for the S/L sample prepared by 1:1 ACN-LAG (sample 13 in Table S4.1), λ = 0.708 Å: (left) film representation; (right) XRD patterns at selected temperatures: T = 37 °C – **1:1 S/L pol I** and **1:1 S/L pol II**; T = 109 °C – **1:1 S/L pol II**; and T = 139 °C – **2:3 S/L**

The first example of a variable-temperature *in situ* experiment is presented in Figure 2. The initial sample obtained by 1:1 ACN-LAG contained a mixture of two **1:1** polymorphs: **pol I** and **pol II**. Upon heating the **1:1 S/L pol I** disappeared, leaving only **pol II** in the sample. Upon further heating, the disappearance of the **1:1 S/L pol II** was followed by the emergence of the **2:3 S/L**.

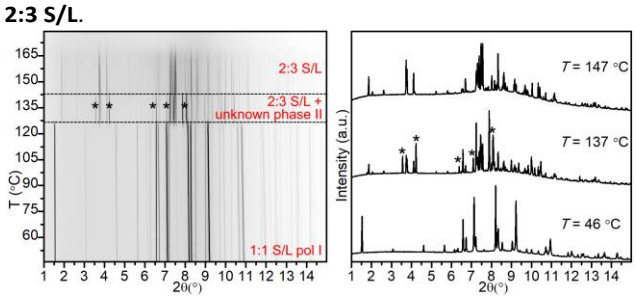

Figure 3. PXRD patterns measured *in situ* upon heating (from 46 to 179 °C, 2 °C/min) for the **S/L** sample prepared by 1:1 EtOH-LAG (sample *5* in Table S4.1), λ = 0.62127 Å: (left) film representation; (right) XRD patterns at selected temperatures: *T* = 46 °C – **1:1 S/L pol I**; *T* = 137 °C – **2:3 S/L** and **unknown phase II**; and *T* = 147 °C – **2:3 S/L**.

The second example of a variable temperature *in situ* experiment is presented in Figure 3. The sample obtained by 1:1 EtOH-LAG reaction initially contained only **1:1 S/L pol I**. Upon heating, the **1:1 S/L pol I** phase disappeared followed by the emergence of the **2:3 S/L** and **unknown phase II**. The **unknown phase II** disappears first upon further heating.

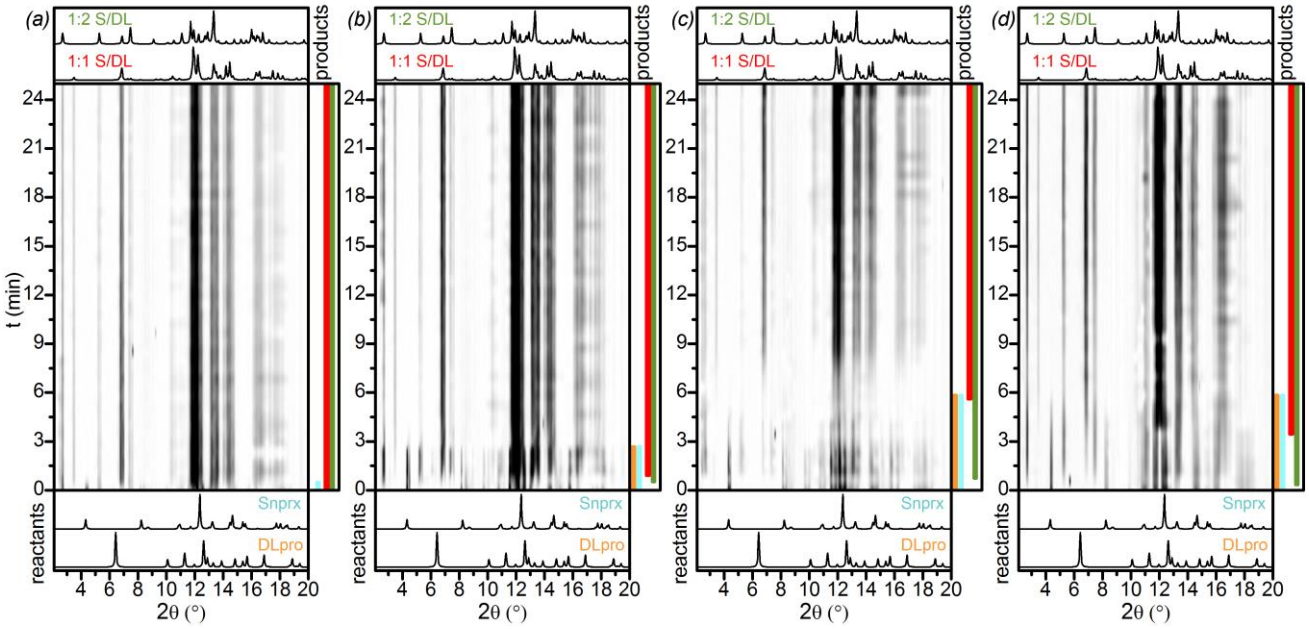

Figure. 4 *In situ* ball-milling X-ray diffraction patterns for the **S/DL** system, λ = 1 Å, 1:1 ratio: (a) MeOH-, (b) EtOH-, (c) ISPN-, and (d) ACN-LAG. Colored bands on the right side of each image represent the presence of phases and are shown only for illustrative purpose.

From the *in situ* variable-temperature PXRD data, it follows that **2:3 S/L** phase must have the highest melting point among the **S/L** cocrystal phases as it is the last phase registered before complete melting (Figs. 2, 3, and S4.1.1). The **1:1 S/L pol I** cocrystal should have a lower melting point than **1:1 S/L pol II** as it disappears first upon heating. However, the exact determination of the melting points of both polymorphs was difficult due to the complexity of the DSC curves (Figs. S4.3.1-S4.3.3)

The possibility of the formation of cocrystal hydrates was checked by performing LAG in the presence of water. No new phases were detected (see samples *17-19* in Table S4.1).

In conclusion, for the **S/L** combination we identified multiple polymorphs and stoichiometrically diverse cocrystals (1:1, 1:2, and 2:3). *In situ* ball-milling revealed the presence of intermediate phases that differed depending on the solvent used, even though the final reaction product was the same. Variable-temperature *in situ* PXRD provided insight into the stability of various forms upon heating, with the **1:1 S/L pol I** being the least thermally stable, and the **2:3 S/L** having the highest thermal stability among the **S/L** forms.

S-naproxen/D-proline (S/D)

S/D system turned out to be the simplest: only one **1:1 S/D** cocrystal, whose structure has already been reported[28] (CCDC REF FEVZOX[28]), was detected in our experiments (see Table S5.1 for the summary of performed experiments). Since preliminary laboratory experiments did not yield any new forms, we decided not to explore this combination any further. However, we accept the possibility that other cocrystal forms may emerge if screening conditions are changed, e.g., if other cocrystallization techniques are used, but this aspect goes beyond the scope of the present work.

S-naproxen/DL-proline

S/DL system yielded several forms: one cocrystal with the 1:1 stoichiometry, one with the 1:2 stoichiometry, and one 1:1 cocrystal hydrate (see Scheme 1). Laboratory LAG experiments (see Table S9.1) showed that varying the solvent in LAG hardly affected the reaction outcome: MeOH-, EtOH-, ISPN-, and ACN-LAG reactions led to the same products: 1:1 LAG reactions resulted in **1:1 S/DL** as the main product and both the **1:2 S/DL** and **1:1 S/DL/H_2O** phases as impurities; 1:2 LAGs gave only **1:2 S/DL** without significant amounts of impurities; in 2:1 LAGs, we

observed mainly **1:1 S/DL** and unreacted **S-nprx**; and finally 2:3 LAGs resulted in mixtures of the **1:1 S/DL** and **1:2 S/DL** phases. These results were in agreement with the *in situ* ball-milling experiments (Fig. 4). All the *in situ* monitored reactions in the presence of the aforementioned four solvents led to (**1:1 S/DL** + **1:2 S/DL**) mixtures (samples *5-8* in Table S3.1). In the MeOH-LAG the **1:2 S/DL** and the **1:1 S/DL** phases seem to start emerging approximately at the same time (Figs. 4a and S3.1.15). In the EtOH-LAG sample, the **1:2 S/DL** clearly starts emerging slightly earlier than the **1:1 S/DL** (Figs. 4b and S3.1.16). Finally, the ISPN- and ACN-LAG samples clearly show that the **1:2 S/DL** emerges first and the **1:1 S/DL** phase appears later (starting from the 5-6th min of reaction) (Figs. 4c and d). These results indicate that the **1:2** form is more kinetically favorable than the **1:1** form. However, both the **1:2 S/DL** and **1:1 S/DL** are relatively stable and, therefore, once formed, do not undergo further conversion (or the rate of conversion is very low), which explains why the final powders after grinding contain both those phases in significant amounts. As was shown in our previous work[41], solvent can affect the reaction rate, which is why it takes longer for the initial reactants to react in ACN- and ISPN-LAG than in MeOH- and EtOH-LAG reactions: the initial reactants stay until the 5-6th min in ACN- and ISPN-LAG reactions, whereas they completely disappear already by the 2nd and 4th min in MeOH- and EtOH-LAG, respectively. Performing reactions in the presence of various solvents to vary the reaction rate helps establishing the order in which the reaction products emerge: in our particular case, slow ACN- and ISPN-LAGs showed the most clearly that the **1:2 S/DL** phase is more kinetically favored than the **1:1 S/DL** under grinding conditions.

As many of the laboratory grinding experiments for this system yielded multiphase samples, we performed variable-temperature *in situ* synchrotron X-ray diffraction measurements for selected powders in order to establish relative stabilities of the phases and their behavior upon heating. All the selected samples behaved in a similar manner (samples *1*, *9*, *11*, and *13* in Table S9.1). Figure 5 demonstrates one of the examples: a sample prepared by 1:1 MeOH-LAG, which initially contained a mixture of **1:1 S/DL**, **1:2 S/DL**, and **1:1 S/DL/H$_2$O** (other examples can be found in Figs. S9.1.1-S9.1.3). When the sample is subjected to heating, first the **1:1 S/DL/H$_2$O** impurity disappears followed by the disappearance of the **1:1 S/DL** phase, which leaves pure **1:2 S/DL** until it melts around 170°C, thereby showing that the latter is the most thermally stable among the **S/DL** phases.

Water-assisted grinding favors the formation of the **1:1 S/DL/H$_2$O** phase (samples *17-20* in Table S9.1). As was mentioned above the presence of this phase was also observed in other laboratory LAG experiments (see Fig. S9.1.4 for the comparison of the 1:1 MeOH- and water-LAG reaction products).

In order to understand how the hydrated **S/DL** form will behave upon heating, we performed variable-temperature *in situ* synchrotron PXRD. We did not observe any new phases. Upon heating, the disappearance of the **1:1 S/DL/H$_2$O** was followed by the emergence of a (**1:1** + **1:2 S/DL**) mixture, which upon further heating exhibited the same behavior as the other measured samples: the **1:1 S/DL** phase melted before the **1:2 S/DL** (Fig. 6).

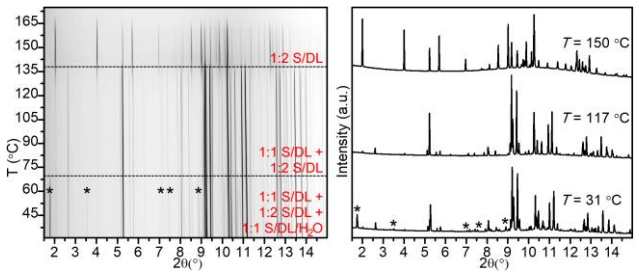

Figure 5. PXRD patterns measured *in situ* upon heating (from 31 to 175 °C, 2 °C/min) for the **S/DL** sample prepared by 1:1 MeOH-LAG (sample *1* in Table S9.1), λ = 0.77663 Å: (left) film representation; (right) XRD patterns at selected temperatures: *T* = 31 °C – **1:1 S/DL**, **1:2 S/DL**, and **1:1 S/DL/H$_2$O** (marked as '*'); *T* = 117 °C – **1:1 S/DL** and **1:2 S/DL**; and *T* = 150 °C – **1:2 S/DL**.

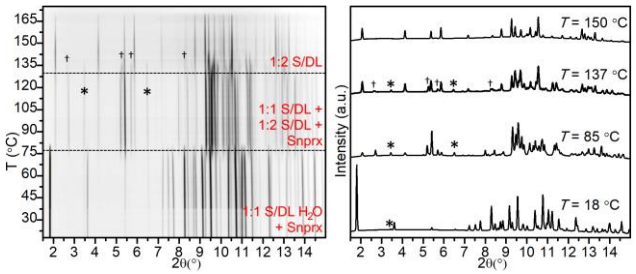

Figure 6. PXRD patterns measured *in situ* upon heating (from 18 to 175 °C, 2 °C/min) for the **S/DL** sample prepared by 1:1 water-LAG (sample *17* in Table S9.1), λ = 0.798 Å: (left) film representation; (right) XRD patterns at selected temperatures: *T* = 18 °C – **1:1 S/DL/H$_2$O** and **S-nprx** (marked as '*'); *T* = 85 °C – **1:1 S/DL**, **1:2 S/DL**, and **S-nprx**; and *T* = 150 °C – **1:2 S/DL**.

We thus conclude that the **S/DL** system was also stoichiometrically diverse, showing 1:1 and 1:2 cocrystals. Water-LAG led to the formation of a cocrystal hydrate. *In situ* ball-milling experiments revealed that the **1:2 S/DL** phase is more kinetically favored under those conditions and emerges before the **1:1 S/DL** (the reaction rate depends on the solvent used). Finally, the *in situ* variable temperature experiments showed that the **1:2 S/DL** has the highest thermal stability and melts the last among the **S/DL** phases.

RS-naproxen/L-proline (RS/L)

As shown in Scheme 1, we found 6 cocrystals for the **RS/L** system: three 1:1 polymorphs, one 1:2 cocrystal, one 1:1 cocrystal hydrate, and one 1:1 cocrystal methanol solvate.

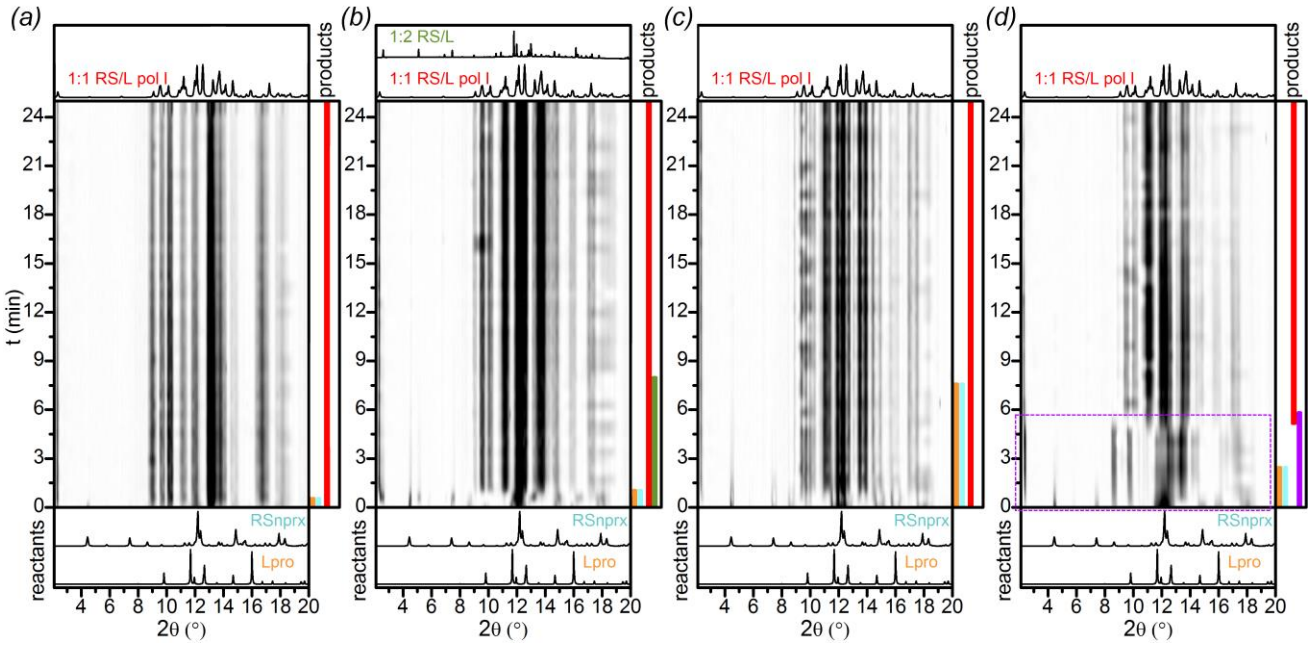

Figure. 7 *In situ* ball-milling X-ray diffraction patterns for the **RS/L** system, λ = 1 Å, 1:1 ratio: (a) MeOH-, (b) EtOH-, (c) ISPN-, and (d) ACN-LAG. Colored bands on the right side of each image represent the presence of phases and are shown only for illustrative purpose; the area outlined by purple in (*d*) shows the presence of the **unknown phase IV**

The analysis of laboratory LAG experiments showed that the reaction outcome is solvent-dependent: 1:1 MeOH-, EtOH-, and ISPN-LAG resulted in the **1:1 RS/L pol I** cocrystal, whereas ACN-LAG led to the **1:1 RS/L pol II** (samples *1*, *5*, *9*, *13* in Tables S6.1 and S7.1). When the initial ratio of the components in laboratory EtOH- and ISPN-LAG was taken so that **pro** was present in an excess amount (1:2 or 2:3 **nprx** : **pro** ratio), the final powders, besides the **1:1 RS/L pol I** also contained the **1:2 RS/L** phase (see samples *6*, *8*, *10*, and *12* in Tables S6.1 and S7.1). Varying the ratio between the components in MeOH- and ACN-LAG reactions, led to the **1:1 RS/L pol I** or **1:1 RS/L pol II**, respectively, and some of the initial material as impurity (see samples *2-4* and *14-16* in Tables S6.1 and S7.1), except 2:3 ACN-LAG reaction (sample *16* in Table S7.1) where the presence of the **1:2 RS/L** as a coproduct was detected as well. Hence, the **1:1 RS/L pol II** was detected only in the ACN-LAG reactions; **1:2 RS/L** was observed mainly in the ISPN- and EtOH-LAG, often as a coproduct of the **1:1 RS/L pol I**.

The results of the *in situ* ball-milling experiments for this system (Fig. 7) differed from our laboratory LAG reactions: grinding with all four tested solvents led to the formation of the **1:1 RS/L pol I** phase, showing no traces of the **1:1 RS/L pol II** even in ACN-LAG, which in the laboratory experiments always resulted in the **1:1 RS/L pol II** (samples *9-12* in Table S3.1). Distinguishing between the two **1:1** polymorphs was complicated due to their close diffraction patterns. In order to be sure that we do not have the **pol II** in the final powders we remeasured PXRD data for those samples at the laboratory diffractometer (Fig. S3.1.11): all the four samples after 1:1 MeOH-, EtOH-, ISPN- and ACN-LAG reactions contained only the **1:1 RS/L pol I**.

MeOH- and ISPN-LAG *in situ* ball-milling showed the formation of only the **1:1 RS/L pol I** (Figs. 7a, d and S3.1.5, S3.1.7). These two reactions differed only by the reaction rate, which was slower in the case of ISPN-LAG (in the latter, the initial reactants disappeared only be the 6th min of reaction against less than by the 1st min in the case of MeOH-LAG).

In situ EtOH-LAG showed the emergence and then disappearance of the **1:2 RS/L** phase at the early stage of reaction (Figs. 7b and S3.1.6). Moreover, ACN-LAG revealed the emergence of another unknown phase (**unknown phase IV**) whose diffraction pattern did not correspond to any previously identified phases (Figs. 7c and S3.1.8). Unfortunately, due to poor quality of the data, reliable determination of this phase was impossible.

Hence, *in situ* ball-milling data showed that the reaction pathway differs depending on the solvent used. Since the results were inconsistent with the preliminary laboratory grinding experiments, we conclude that the reaction is highly sensitive to the milling conditions, which renders a direct comparison of the laboratory grinding and *in situ* ball-milling unreliable in this case.

Additional *in situ* ball-milling experiments were performed for the 1:2 MeOH- and ISPN-LAG reactions (samples *13* and *14* in Table S3.1) in order to monitor the formation of the **1:2 RS/L**. Unfortunately, the MeOH-LAG data had a very poor quality and we were able only to collect the PXRD pattern of the final powder, which showed no presence of **1:2 RS/L**, only **1:1 RS/L pol I** and initial compounds as impurities (Fig. S3.1.10). The ISPN-LAG, on the other hand, clearly showed the formation of the **1:2 RS/L**, that started emerging later (around the 4th min of reaction) than the **1:1 RS/L pol I** (which was observed already after 1 min). The final powder contained both the **1:1 RS/L pol I** and **1:2 RS/L** (Figs. S3.1.9 and S3.1.18). These two results were consistent with our laboratory data, in which the formation of the **1:2 RS/L** phase was observed only in ISPN-LAG (sample *10* in Tables S6.1 and S7.1), whereas 1:2 MeOH-LAG showed no traces of this phase, but only the **1:1 RS/L pol I** (sample *2* in Tables S6.1 and S7.1).

Variable temperature *in situ* PXRD helped structure determination of the **1:2 RS/L** phase providing access to its pure diffraction pattern (Fig. 8). The **1:2 RS/L** phase was always obtained in a mixture with other phases and thus indexing and structure determination were tricky at ambient conditions. The variable temperature experiment showed that the **1:2 RS/L** phase is more stable upon heating and thus disappears later than the **1:1 RS/L pol I**: the sample in the temperature range from 127 to 144 °C contained almost pure **1:2 RS/L** (the amount of **L-pro** was negligible).

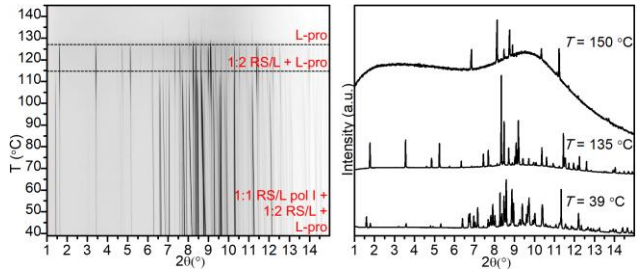

Figure 8. PXRD patterns measured *in situ* upon heating (from 39 to 163 °C, 2 °C/min) for the **RS/L** sample prepared by 1:2 ISPN-LAG (sample *10* in Table S7.1), λ = 0.708 Å: (left) film representation; (right) XRD patterns at selected temperatures: *T* = 39 °C – **1:1 RS/L pol I**, **1:2 RS/L**, and **L-pro**; *T* = 135 °C – **1:2 RS/L** and **L-pro**; and *T* = 150 °C – **L-pro**.

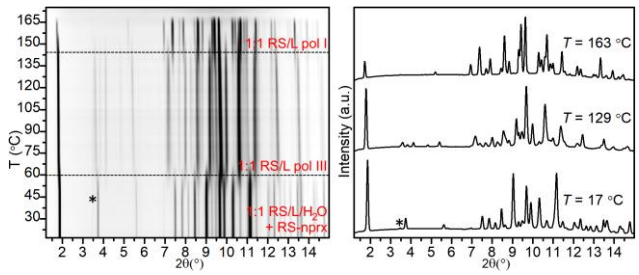

Figure 9. PXRD patterns measured *in situ* upon heating (from 17 to 175 °C, 2 °C/min) for the RS/L sample prepared by 1:1 water-LAG (sample 17 in Table S7.1), λ = 0.78487 Å: (left) film representation; (right) XRD patterns at selected temperatures: *T* = 17 °C – **1:1 RS/L/H$_2$O**, **RS-nprx** (marked as '*'); *T* = 129 °C – 1: 1 RS/L pol III; and *T* = 163 °C – **1:1 RS/L pol I**.

Water-LAG in this system yielded already known **1:1 RS/L/H$_2$O** cocrystal hydrate (CCDC REF BEXGUI[28], samples *17-19* in Tables S6.1 and S7.1). Using variable-temperature *in situ* PXRD for this sample we found another polymorph – **1:1 RS/L pol III** (Fig. 9), which was not observed in any other LAG experiments. This new **pol III** emerged upon heating when water evaporated from the initial hydrated sample; upon further heating **pol III** disappeared followed by the appearance of the **1:1 RS/L pol I**. From the structural point of view, the **1:1 RS/L/H$_2$O** and **1:1 RS/L pol III** exhibit completely different types of packing (the former being of the Type I and the latter of Type II, (see Structural analysis section for the description of the packing types and Fig. S10.2 for the comparison of this particular case), thereby showing that water evaporation from the hydrated **1:1 RS/L/H$_2$O** cocrystals induces an entire structural rearrangement, leading the cocrystal with a completely different structural type than other cocrystal forms from this system (which all exhibit the Type I packing).

In conclusion, the **RS/L** system exhibits cocrystals with various stoichiometries (1:1 and 1:2), including a hydrate and a solvate. *In situ* ball-milling showed that LAG reactions are highly sensitive to the solvent used as well as the experimental setup and also revealed that even if the final product is the same, the reaction pathway is solvent-dependent. Variable-temperature *in situ* PXRD data helped determining the structure of the **1:2 RS/L** phase and gave access to the **1:1 RS/L pol III** that was not observed under any other conditions.

RS-naproxen/DL-proline

For the **RS/DL** system we found two polymorphs with the 1:1 stoichiometry – **1:1 RS/DL pol I** and **1:1 RS/DL pol II**, – and one **1:1 RS/DL/H$_2$O** cocrystal hydrate (the structure of the cocrystal hydrate was previously reported, CCDC BEYTUW[28]). We also established the formation of the **(1:2 R/DL + 1:2 S/DL)** conglomerate under certain conditions (Scheme 1).

In general, the laboratory LAG experiments mainly yielded the **1:1 RS/DL pol I** cocrystal (Table S8.1). The formation of the conglomerate was observed when the initial **RS-nprx** and **DL-pro** were ground in 1:2 or 2:3 ratio, often as a coproduct of the **1:1 RS/DL pol I** phase (samples *2*, *4*, *6*, *8*, *10*, *12*, *14*, *16* in Table S8.1); the presence of the **(1:2 R/DL + 1:2 S/DL)** conglomerate was also detected in the 1:1 ISPN-LAG (sample *9* in Table S8.1). The fact that we dealt exactly with the conglomerate and not any other combination of phases was confirmed by variable-temperature *in situ* PXRD. The sample obtained by 1:2 MeOH-LAG was heated in a capillary. Initially, the sample contained a mixture of different phases: **1:1 RS/DL pol I**, **(1:2 R/DL + 1:2 S/DL)** conglomerate, and **DL-pro monohydrate**. Upon heating, first **DL-pro monohydrate** transformed into unhydrated **DL-pro**, which upon further heating disappeared along with **1:1 RS/DL pol I** phase, leaving only the pure **conglomerate** (Fig. 10). The *in situ* variable temperature PXRD data are in agreement with the DSC, which show that the melting point of the **1:1 RS/DL pol I** phase is lower than the eutectic point of the **conglomerate** (152(1) against 168(1)°C, respectively) and thus, the former should melt before the latter.

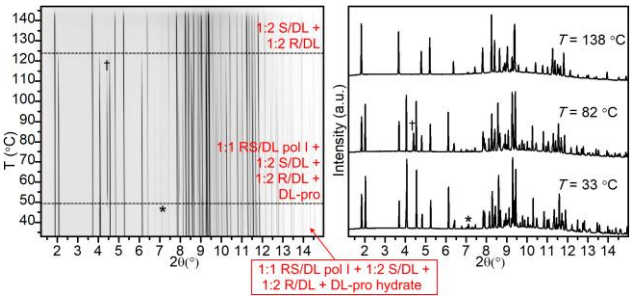

Figure 10. PXRD patterns measured in situ upon heating (from 33 to 147 °C, 2 °C/min) for the **RS/DL** sample prepared by 1:2 MeOH-LAG (sample 2 in Table S8.1), λ = 0.708 Å: (left) film representation; (right) XRD patterns at selected temperatures: T = 33 °C – **1:1 RS/DL pol I**, **(1:2 R/DL + 1:2 S/DL)** conglomerate, and DL-pro monohydrate; T = 82 °C – 1:1 RS/DL pol I, **(1:2 R/DL + 1:2 S/DL)** conglomerate, and DL-pro; and T = 138 °C – **(1:2 R/DL + 1:2 S/DL)** conglomerate.

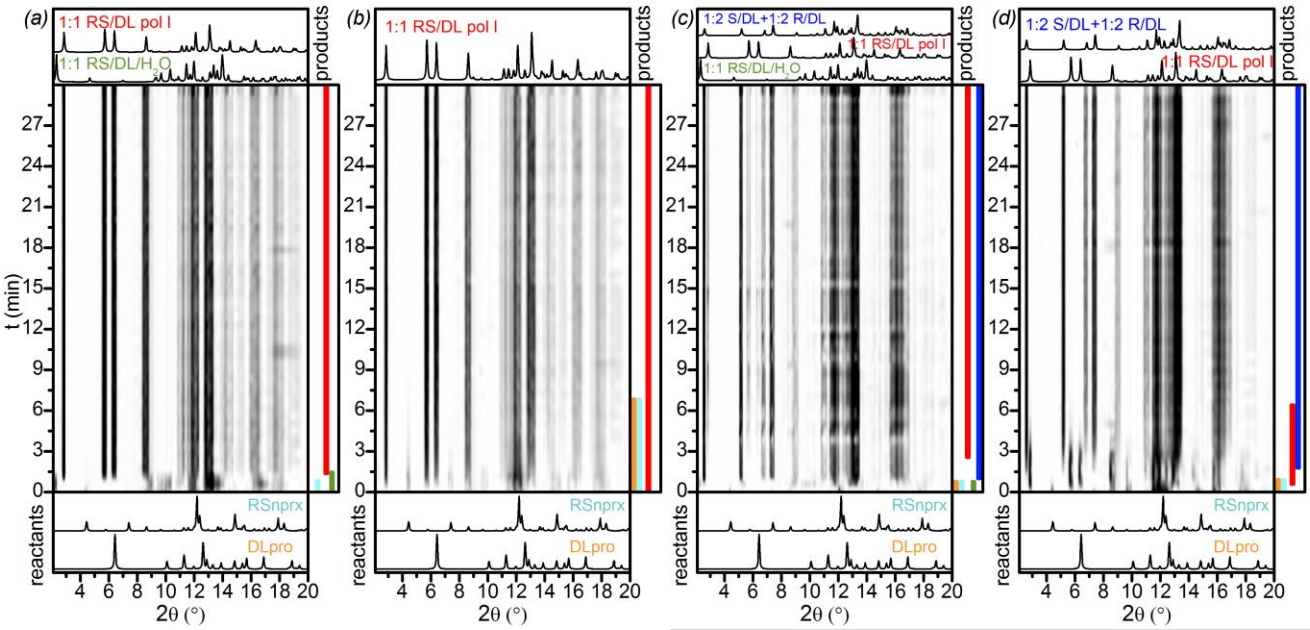

Figure 11. *In situ* ball-milling X-ray diffraction patterns for the **RS/DL** system, λ = 1 Å: (a) 1:1 MeOH-, (b) 1:1 ISPN-, (c) 1:2 MeOH-LAG and (d) 1:2 ISPN-LAG. Colored bands on the right side of each image represent the presence of phases and are shown only for illustrative purpose.

In situ 1:1 ball-milling, neither in the presence of MeOH nor ISPN, showed conglomerate formation (samples *15* and *16* in Table S3.1). ISPN-LAG led directly to the **1:1 RS/DL pol I** phase (Fig. 11b). MeOH-LAG revealed **1:1 RS/DL/H_2O** emerging at the beginning of the reaction and then disappearing shortly (Figs. 11a and S3.1.12).

On the other hand, when the ratio was changed for 1:2, *in situ* ball-milling in the presence of both MeOH and ISPN showed the formation of the **conglomerate** (samples *17* and *18* in Table S3.1). In 1:2 MeOH-LAG, the final powder contained both the **conglomerate** and the **1:1 RS/DL pol I**: the **conglomerate** started to emerge first and the **1:1** phase followed (Fig. 11c and S3.1.13); moreover, we detected again the formation of the **1:1 RS/DL/H_2O** within the 1st min of reaction, which later disappeared. In 1:2 ISPN-LAG, the final sample contained only the **conglomerate**, whose emergence was preceded by the **1:1 RS/DL pol I** phase, which disappeared already after 8 min of grinding (Fig. 11d and S3.1.14). These experiments show that the conglomerate and the **1:1 RS/DL pol I** phase kinetically compete with each other and the result significantly depends on the reaction conditions.

Water-assisted laboratory grinding yielded the **1:1 RS/DL/H_2O** cocrystal hydrate (samples *17-19* Table S8.1), which upon heating transformed into the **1:1 RS/DL pol II** phase when water evaporated from the sample. Upon further heating the **1:1 RS/DL pol II** simply melted without any other phases emerging (Fig. 12). The **1:1 RS/DL pol II** cocrystal was not detected upon any other tested conditions. Comparing **1:1 RS/DL/H_2O** and **1:1 RS/DL pol II** showed that the hydrated structure undergoes a complete structural rearrangement upon heating, with the final unhydrated structure being of the Type II packing, unlike the initial hydrated form and the **1:1 RS/DL pol I** cocrystal both belonging to the Type I packing (see Structural analysis section for the description of the packing types and Fig. S10.3 for the comparison of this particular case).

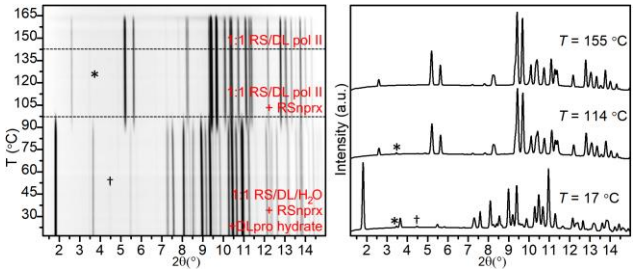

Figure 12. PXRD patterns measured *in situ* upon heating (from 17 to 170 °C, 2 °C/min) for the **RS/DL** sample prepared by 1:1 water-LAG (sample 17 in Table S8.1), λ = 0.78487 Å: (left) film representation; (right) XRD patterns at selected temperatures: T = 17 °C – **1:1 RS/DL/H_2O**, **RS-nprx** (marked as '*'), and **DL-pro monohydrate** (marked as '†'); T = 114 °C – **1:1 RS/DL pol II** and RS-nprx; and T = 155 °C – **1:1 RS/DL pol II**.

Hence, the most interesting finding for the **RS/DL** system is the formation of the **(1:2 R/DL + 1:2 S/DL)** conglomerate under certain conditions. *In situ* variable-temperature PXRD data were essential to prove this fact as they provided access to the diffraction pattern of the pure conglomerate. Another *in situ* variable-temperature PXRD experiment allowed structure solution of the **1:1 RS/DL pol II**, as this phase was observed only upon heating and not under any other tested conditions.

Structural analysis

In our previously published work[41], we studied the flurbiprofen/proline system, which similarly to **naproxen/proline** showed a great variety of cocrystal phases. Below, we will analyse the structural features of **nprx**/**pro** cocrystals and compare them to those seen in the **flurbiprofen**/**proline** system.

Unlike **flurbiprofen**/**proline** cocrystals, for which we distinguished 4 packing types[41], **nprx**/**pro** cocrystals exhibit less variability–only two types of packing were found (Scheme 2): 1) Type I – sandwich-like type, in which **pro** chains form a center layer with **nprx** attached from both sides; 2) Type II –

layer type, in which one can distinguish alternating layers of **pro** and **nprx**, with **nprx** arranged in a zip-like manner. Moreover, Type I can be divided into two subtypes, *a* and *b*, which differ from one another by the arrangement of **nprx** molecules: in the Ia subtype, **nprx** packs in a herringbone manner and in the II*b* type **nprx** molecules are parallel. Schematic representation of these packing types and illustrating examples are given in Fig. 13.

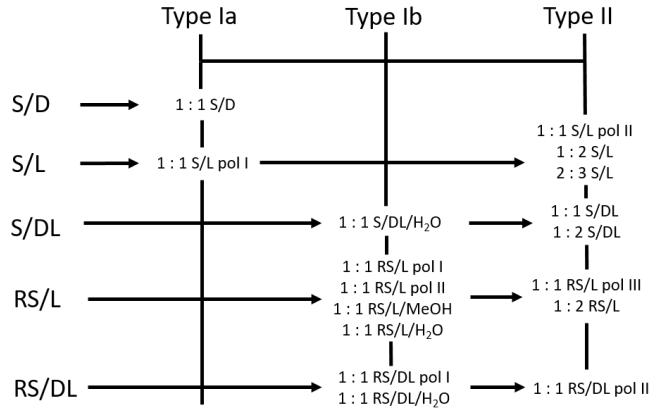

Scheme 2. Structural types distinguished for the **nprx**/**pro** cocrystals

Pro is zwitterionic in all the structures and form head-to-tail chains through charge-assisted N–H…O hydrogen bonds, which are typical of crystalline **pro** and other amino acids.[25–27] **Nprx** attaches to **pro** via O–H…O hydrogen bonds between the carboxyl group and carboxylate, respectively.

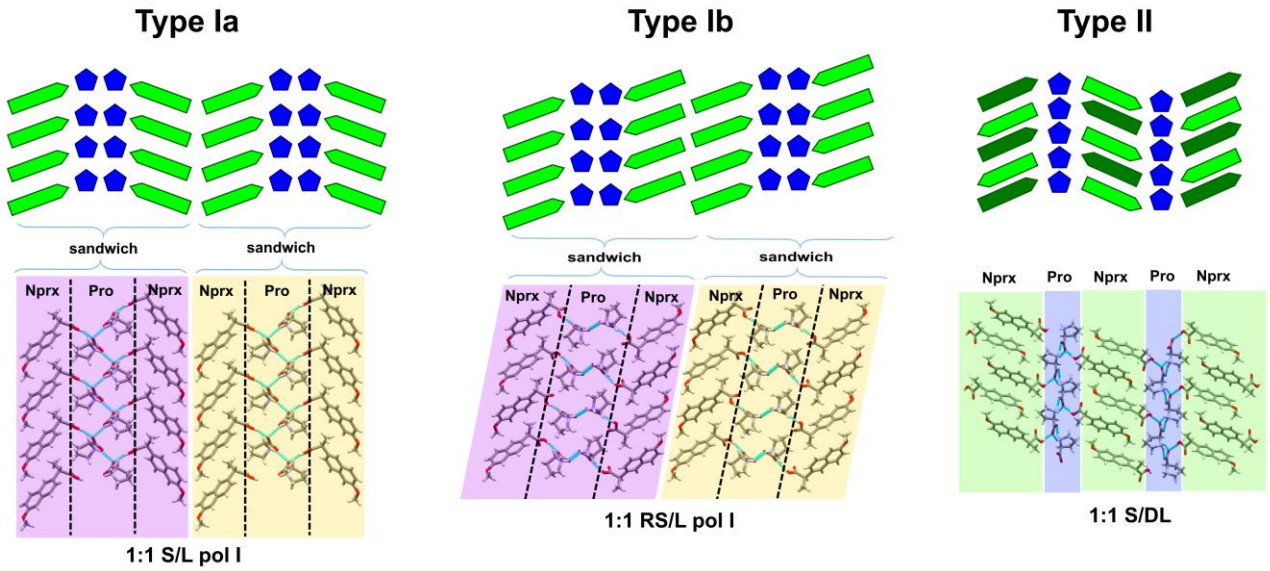

Figure 13. Schematic representation of the structural types distinguished for the **nprx**/**pro** system. Blue pentagons and green pointed (the COOH group orientation) rectangles represent **pro** and **nprx** molecules, respectively. Type I is the sandwich-like type, separate sandwiches are colored pink and yellow in the structure examples; Type II is the layer type: alternating **nprx** and **pro** layers are colored green and blue, respectively, in the structure example.

The fact that **nprx**/**pro** cocrystals vary less in their structural features than flurbiprofen/proline cocrystals may be related to the structural peculiarities of **nprx** and flurbiprofen themselves. Pure **flurbiprofen** exhibits polymorphism (CCDC FLUBIP[58] (*P*-1) and FLUBIP02[59] ($P2_1/n$)) and we found that the packing in cocrystal structures resembled that of pure **flurbiprofen**, whereas in the case of **nprx**, no polymorphism has been reported so far. Both racemic and enantiopure **nprx** structures exhibit a similar general packing motif: **nprx** dimers are arranged in a stacking manner to enable efficient π-π overlap between the benzene rings. **S-nprx/ethanol** solvate, which we obtained from ethanol solution, also exhibited the same packing motif as non-solvated **nprx**, with ethanol molecules "wedged" in between **nprx** dimers (see Fig. S10.1). Since ethanol was essential to keep the structure together, the latter turned out to be very unstable if exposed to air. Thus, pure **nprx** is less prone to polymorphism and thus results in a fewer variants of packing in cocrystals, in comparison with flurbiprofen.

Previously reported cocrystals of **nprx** and amino acids[17] also demonstrated the same types of packing: **nprx**/alanine (CCDC RODSEK and RODSIO[17]) and **nprx**/tryptophan (CCDC RODSOU[17]) had the sandwich-like type (I) and **nprx**/tyrosine (CCDC RODSUA[17]) exhibited the layer type (II) packing. Hence, we suspect that, since **nprx** prefers a stacking manner of molecular arrangement, the weak interactions between its bulky molecules are responsible for the overall packing of **nprx**/amino acid cocrystals.

At the same time, we believe that amino acid chains, with strong charge-assisted hydrogen bonds between molecules, should provide the structure with additional stability and a higher melting point in comparison with the structure of the initial API as the percentage of strong interactions in the structure increases. For instance, the melting point of flurbiprofen/proline cocrystals was minimum 30 °C higher in comparison with pure **flurbiprofen** (T_m (**racemic flurbiprofen**) = 115 °C, T_m (enantiopure **flurbiprofen**) = 109 °C)[41]. The melting points of some of the **nprx**/**pro** cocrystals were also found to be higher than that of pure **nprx** (see Table 1). The highest melting points were observed for the cocrystals with the 1:2 and 2:3 stoichiometries, which can be explained by the fact that these cocrystals exhibit a higher percentage of

charge-assisted hydrogen bonds as compared with the 1:1 phases due to an extra **pro** molecule in the asymmetric unit. The 1:1 phases on the other hand were found to have melting points very close to pure **nprx**, which highlights the fact that the interactions between **nprx** molecules themselves are substantial and provide efficient bonding even without strong-charge assisted hydrogen bonds.

Table 1. Determined melting points of the initial API and its cocrystals with **pro**

Compound	Melting point, °C
S-nprx	155(1)
RS-nprx	153(1)
2:3 S/L	181(1)
1:1 S/D	155(1)
1:1 RS/L pol I	162(1)
1:1 RS/L pol II	159(1)
1:2 RS/L	171(1)
1:1 RS/DL pol I	152(1)
1:2 S/DL	182(1)
(1:2 S/DL + 1:2 R/DL)	168(1) – eutectic point

Another peculiar finding about **nprx**/**pro** cocrystals is the cocrystals of the 1:2 and 2:3 stoichiometries, in which **nprx** is connected only to one or two **pro**, respectively, and the rest **pro** molecules in the asymmetric unit are connected to themselves. In Scheme 3 we present four possibilities of the interactions between **nprx** and **pro** in an asymmetric unit. All the five combinations of racemic and/or enantiopure **nprx** and **pro** yielded at least one 1:1 stoichiometry cocrystal, case (*a*) in Scheme 3. Cocrystals of this type were seen in abundance in both the **nprx**/**pro** and **flurbiprofen**/**pro** systems. A cocrystal of the 1:2 stoichiometry, case (*b*) in Scheme 3, was also observed in the **flurbiprofen**/**pro** system (CCDC VEVLAM[41]) and it turns out that its structure is very similar to the 1:2 **nprx**/**pro** cocrystals: two perpendicularly going infinite **pro** chains form a **pro** layer, in which **nprx** is connected only to one of those chains (see Fig. S10.4). In the **2:3 S/L** cocrystal, case (*c*) in Scheme 3, the **pro** layer is comprised of clusters situated one on top of another and made of three interconnected **pro** chains; **nprx** is attached to only two chains from the cluster (see Fig. S10.5). The last type of interactions, case (*d*), in which one pro molecule attaches two APIs via two O-H…O hydrogen bonds formed by its carboxylate group with two carboxyl groups of an API resulting in the cocrystals with the 2:1 (**API**:**pro**) stoichiometry, was not observed in the **nprx**/**pro** system, even though it was very common among the **flurbiprofen**/**pro** cocrystals.

Cocrystals with the aforementioned 1:2 and 2:3 stoichiometries are less common. Their existence shows that in order to obtain a cocrystal of desired stoichiometry it is not enough to simply choose the compounds with potential binding sites, but it is also important to consider the possibility of other potentially stronger interactions that might occur between the molecules of one kind, like in this case, when instead of binding a second **nprx** to the available oxygen of the carboxylate, **pro** preferred to bind another symmetrically nonequivalent **pro** molecule and form a 1:2 or 2:3 (**nprx** : **pro**) cocrystal.

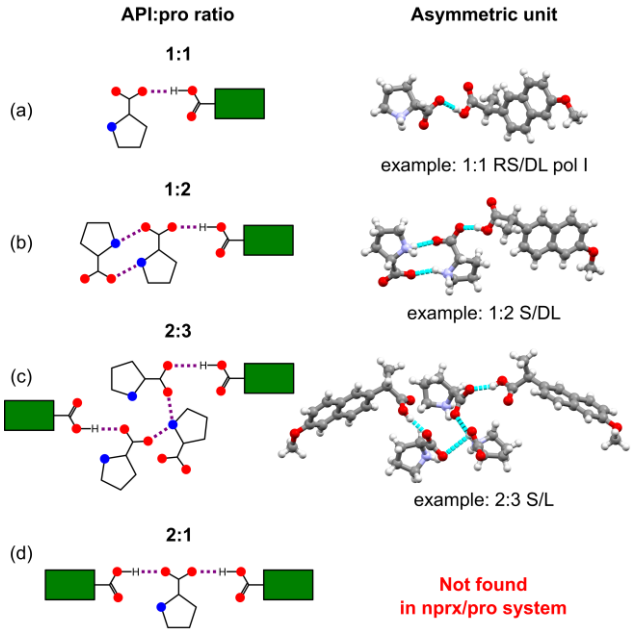

Scheme 3. Four possibilities of interactions between profen (API) and proline molecules in an asymmetric unit of their cocrystals. (*a*), (*b*), and (*c*) cases are observed in the **nprx**/**pro** system; (d) case, typical of the **flurbiprofen**/**pro** system, was not detected for **nprx**/**pro**. Red circles represent oxygen atoms, blue circles represent nitrogen, green rectangles with attached -COOH group represent a profen molecule (API).

Conclusions

Nprx/**pro** system exhibits a wide variety of cocrystal forms: 17 in total, whose structures were determined, plus four unknown phases whose structures were impossible to find. Similarly to the previously reported case of flurbiprofen/proline cocrystals[41], we believe that the complexity of the system can be associated with the following two factors: first, how well the three-dimensional structures of the initial compounds "suit" one another to form an efficient packing pattern; and second, the conformational flexibility of the initial molecules.

As for the first factor, the system might have a higher possibility of efficient packing in the case of racemic initial compounds in comparison with the enantiopure ones because having both enantiomers in the structure may increase the chances of "suitability". At the same time, some of the chiral combinations may form stronger connections than the others. For instance, the **S/D** system showed only one cocrystal, whereas the **S/L** system yielded minimum four cocrystal phases. Probably, in the case of the **S/D** combination, the interactions between coformers are so efficient that they do not leave any chance for other polymorphs or stoichiometrically diverse cocrystals to emerge under studied conditions as the former is both thermodynamically and kinetically favored; whereas in the **S/L** system, the initial coformers might fit one another to a lesser degree and, thus, many competitive phases (probably of approximately the same energies) may emerge. This conclusion is speculative on our part, and we suggest that a careful calculation of the relative energies of the obtained cocrystals can shine more light on this chirality-related aspect of cocrystallization.

As for the second factor, **pro** has been known for its conformational flexibility[60], moreover we found two polymorphs of **L-pro** itself in the Cambridge Structural Database[61] (CCDC PROLIN[50] and PROLIN04[41]). Hence, we believe that the conformational flexibility of **pro** can partly be responsible for the found polymorphic and stoichiometric diversity of the **nprx**/**pro** cocrystals.

The melting points that we were able to determine for several **nprx**/**pro** cocrystals turned out to be higher than that of pure **nprx**, which is due to the **pro**'s ability to form charge-assisted hydrogen bonded chains owing to which the percentage of strong interaction in the structure increases in comparison with the pure API. As all amino acids in the crystalline state are zwitterionic and tend to form such chains[25–27], which are also frequently observed in their cocrystals[17,28,62], this structural feature of amino acid cocrystals can be especially useful when handling unstable APIs: one of the reported examples is the improvement of the stability of highly hygroscopic lactic acid, via its cocrystallization with tryptophan.[29]

In situ ball-milling monitored by synchrotron X-ray diffraction has already proved vital for studying solid-state reactions.[63–67] In the current study, we used this method to verify the possibility of intermediate phases in our LAG reactions. We detected several intermediate phases emerging in the course of reaction. We found that the reaction pathway can be solvent dependent, as for instance, in the case of the **S/L** system, when in the beginning of the reaction we observed different phases depending on the solvent used, even though the final product was the same. Knowing at which moment to stop the reaction in order to obtain a desired product (for instance, one of the intermediates) can provide a better control of the reaction outcome.

Synchrotron X-ray diffraction data turned out to be indispensable when dealing with complicated product mixtures. Similarly to our work on flurbiprofen/proline cocrystals, synchrotron X-ray diffraction data collected *in situ* upon heating allowed direct monitoring of phase changes, and gave access to the pure PXRD patterns of certain phases. They allowed structure solution of the **1:2 RS/L** cocrystal, otherwise observed only in mixture, helped us to confirm the conglomerate formation in the **RS/DL** system, and revealed the **1:1 RS/DL pol II** and **1:1 RS/L pol II** phases that emerged when the hydrated forms of the corresponding cocrystals were heated and water evaporated.

The results of this work should be of great interest to pharmaceutical industry as they deal with various chirality aspects of cocrystallization of APIs, provide insight into various structural features of cocrystals with zwitterionic coformers via the example of **pro**, and demonstrate how clever combining various state-of-the-art characterization methods helps not only identify existing phases but also provides means for a better control of solid-state reactions.

Conflicts of interest

There are no conflicts to declare.

Acknowledgements

The authors thank Universite catholique de Louvain and FNRS (FRIA scholarship allocated to N. Tumanova) for financial support. We thank ESRF, PSI, BESSY II, and SOLEIL for the beam time allocation. We thank the PC^2 platform at the University of Namur for single-crystal and powder X-ray diffraction analysis. Natalia Tumanova is grateful to Dr. F. Emmerling's group for a warm welcome during her STSM funded by COST Crystallize Action (CM1402). The authors highly appreciate advices from Dr. Radovan Cerny concerning the structure solution from PXRD. We thank Lisa Baulard for her help in preparing solutions for single crystal growth, Pascal Van Velthem for helping us to treat DSC data, and Jean-François Statsyns for measuring the TGA data.

References

1. A. I. Kitaigorodsky, *Molecular Crystals and Molecules*, Academic Press, 1973.
2. J. Zukerman-Schpector and E. R. T. Tiekink, *Zeitschrift für Krist.*, 2008, **223**, 233–234.
3. W. Jones, W. D. S. Motherwell, and A. V. Trask, *MRS Bull.*, 2011, **31**, 875–879.
4. H. G. Brittain, *J. Pharm. Sci.*, 2013, **102**, 311–7.
5. N. Schultheiss and A. Newman, *Cryst. Growth Des.*, 2009, **9**, 2950–2967.
6. A. N. Sokolov, T. Friscić, and L. R. MacGillivray, *J. Am. Chem. Soc.*, 2006, 128, 2806–2807.
7. M. C. Etter, G. M. Frankenbach, and D. A. Adsmond, *Mol. Cryst. Liq. Cryst. Inc. Nonlinear Opt.*, 1990, **187**, 25–39.
8. M. Morimoto, S. Kobatake, and M. Irie, *Chem. Commun.*, 2008, **121**, 335–337.
9. A. Carletta, F. Spinelli, S. d'Agostino, B. Ventura, M. R. Chierotti, R. Gobetto, J. Wouters, and F. Grepioni, *Chem. - A Eur. J.*, 2017, **23**, 5317–5329.
10. V. Ramamurthy and Y. Inoue, *Supramolecular photochemistry : controlling photochemical processes*, Wiley, 2011.
11. L. A. Nguyen, H. He, and C. Pham-Huy, *Int. J. Biomed. Sci.*, 2006, **2**, 85–100.
12. T. Friščić, L. Fábián, J. C. Burley, W. Jones, and W. D. S. Motherwell, *Chem. Commun.*, 2006, 5009–5011.
13. T. Friščić and W. Jones, *Faraday Discuss.*, 2007, **136**, 167–178.
14. N. Takata, K. Shiraki, R. Takano, Y. Hayashi, and K. Terada, *Cryst. Growth Des.*, 2008, **8**, 3032–3037.
15. P. Thorey, P. Bombicz, I. M. Szilágyi, P. Molnár, G. Bánsághi, E. Székely, B. Simándi, L. Párkányi, G. Pokol, and J. Madarász, *Thermochim. Acta*, 2010, **497**, 129–136.
16. G. Springuel, B. Norberg, K. Robeyns, J. Wouters, and T. Leyssens, *Cryst. Growth Des.*, 2012, **12**, 475–484.
17. N. Tumanova, N. Tumanov, K. Robeyns, Y. Filinchuk, J. Wouters, and T. Leyssens, *CrystEngComm*, 2014, **16**, 8185–8196.
18. G. Springuel and T. Leyssens, *Cryst. Growth Des.*, 2012, **12**, 3374–3378.

19. G. Springuel, L. Collard, and T. Leyssens, *CrystEngComm*, 2013, **15**, 7951–7958.
20. J. Mahieux, S. Gonella, M. Sanselme, and G. Coquerel, *CrystEngComm*, 2012, **14**, 103–111.
21. S. Iwama, K. Kuyama, Y. Mori, K. Manoj, R. G. Gonnade, K. Suzuki, C. E. Hughes, P. A. Williams, K. D. M. Harris, S. Veesler, H. Takahashi, H. Tsue, and R. Tamura, *Chemistry*, 2014, **20**, 10343–10350.
22. B. Harmsen and T. Leyssens, *Cryst. Growth Des.*, 2018, **18**, 441–448.
23. M. D. Eddleston, M. Arhangelskis, T. Friščić, and W. Jones, *Chem Commun*, 2012, **48**, 11340–11342.
24. B. Harmsen and T. Leyssens, *Cryst. Growth Des.*, 2018, **18**, 3654–3660.
25. E. Boldyreva, ed. Boeyens J.F. and Ogilvie J.C.A., Springer, 2008, pp. 167–192.
26. S. N. Vinogradov, *Int. J. Pept. Protein Res.*, 1979, **14**, 281–289.
27. C. G. Suresh and M. Vijayan, *Int. J. Pept. Protein Res.*, 2009, **22**, 129–143.
28. A. Tilborg, G. Springuel, B. Norberg, J. Wouters, and T. Leyssens, *CrystEngComm*, 2013, **15**, 3341–3350.
29. J. B. de Maere d'Aertrycke, K. Robeyns, J. Willocq, and T. Leyssens, *J. Cryst. Growth*, 2017.
30. H. He, Y. Huang, Q. Zhang, J. R. Wang, and X. Mei, *Cryst. Growth Des.*, 2016, **16**, 2348–2356.
31. M. Liu, C. Hong, Y. Yao, H. Shen, G. Ji, G. Li, and Y. Xie, *Eur. J. Pharm. Biopharm.*, 2016, **107**, 151–159.
32. I. Nugrahani, D. Utami, S. Ibrahim, Y. P. Nugraha, and H. Uekusa, *Eur. J. Pharm. Sci.*, 2018, **117**, 168–176.
33. I. Nugrahani, D. Utami, B. Permana, and S. Ibrahim, *J. Appl. Pharm. Sci.*, 2018, **8**, 57–63.
34. S. L. Childs, N. Rodríguez-Hornedo, L. S. Reddy, A. Jayasankar, C. Maheshwari, L. McCausland, R. Shipplett, and B. C. Stahly, *CrystEngComm*, 2008, **10**, 856–864.
35. M. R. Shimpi, S. L. Childs, D. Boström, and S. P. Velaga, *CrystEngComm*, 2014, **16**, 8984–8993.
36. C. R. Ramanathan and M. Periasamy, *Tetrahedron: Asymmetry*, 1998, **9**, 2651–2656.
37. X. Hu, Z. Shan, and Q. Chang, *Tetrahedron: Asymmetry*, 2012, **23**, 1327–1331.
38. M. Shyam Sundar, H. R. Talele, H. M. Mande, A. V. Bedekar, R. C. Tovar, and G. Muller, *Tetrahedron Lett.*, 2014, **55**, 1760–1764.
39. X. Qu, J. Lu, C. Zhao, J. F. Boas, B. Moubaraki, K. S. Murray, A. Siriwardana, A. M. Bond, and L. L. Martin, *Angew. Chemie*, 2011, **2**, 1627–1630.
40. O. Shemchuk, B. K. Tsenkova, D. Braga, M. T. Duarte, V. André, and F. Grepioni, *Chem. - A Eur. J.*, 2018.
41. N. Tumanova, N. Tumanov, K. Robeyns, F. Fischer, L. Fusaro, F. Morelle, V. Ban, G. Hautier, Y. Filinchuk, J. Wouters, T. Leyssens, and F. Emmerling, *Cryst. Growth Des.*, 2018, **18**, 954–961.
42. V. G. Rajurkar, R. D. Gite, and V. B. Ghawate, *Anal. Chem. Lett.*, 2015, **5**, 229–238.
43. I. Vayá, M. C. Jiménez, and M. A. Miranda, *Tetrahedron: Asymmetry*, 2005, **16**, 2167–2171.
44. C. F. Macrae, I. J. Bruno, J. A. Chisholm, P. R. Edgington, P. McCabe, E. Pidcock, L. Rodriguez-Monge, R. Taylor, J. van de Streek, and P. A. Wood, *J. Appl. Crystallogr.*, 2008, **41**, 466–470.
45. K. Ravikumar, S. S. Rajan, V. Pattabhi, E. J. Gabe, and IUCr, *Acta Crystallogr. Sect. C Cryst. Struct. Commun.*, 1985, **41**, 280–282.
46. Y. B. Kim, H. J. Song, and I. Y. Park, *Arch. Pharm. Res.*, 1987, **10**, 232–238.
47. M. D. King, W. D. Buchanan, and T. M. Korter, *Phys. Chem. Chem. Phys.*, 2011, **13**, 4250–4259.
48. D. E. Braun, M. Ardid-Candel, E. D'Oria, P. G. Karamertzanis, J.-B. Arlin, A. J. Florence, A. G. Jones, and S. L. Price, *Cryst. Growth Des.*, 2011, **11**, 5659–5669.
49. R. T. K.Manoj, H.Takahashi, H.Tsue, *CSD Private Communication*, 2016.
50. B. K. Kayushina, R.L., Vainshtein, *Krist. (Crystallogr. Rep.)*, 1965, **10**, 833.
51. J. Janczak and P. Luger, *Acta Crystallogr. Sect. C Cryst. Struct. Commun.*, 1997, **53**, 1954–1956.
52. S. Myung, M. Pink, M. H. Baik, and D. E. Clemmer, *Acta Crystallogr. Sect. C Cryst. Struct. Commun.*, 2005, **61**, 506–508.
53. Y. Hayashi, M. Matsuzawa, J. Yamaguchi, S. Yonehara, Y. Matsumoto, M. Shoji, D. Hashizume, and H. Koshino, *Angew. Chemie - Int. Ed.*, 2006, **45**, 4593–4597.
54. S. Padmanabhan, S. Suresh, and M. Vijayan, *Acta Crystallogr. Sect. C Cryst. Struct. Commun.*, 1995, **51**, 2098–2100.
55. O. Paris, C. Li, S. Siegel, G. Weseloh, F. Emmerling, H. Riesemeier, A. Erko, and P. Fratzl, *J. Appl. Cryst*, 2007, **40**, 466–470.
56. A. P. Hammersley, S. O. Svensson, M. Hanfland, A. N. Fitch, and D. Hausermann, *High Press. Res.*, 1996, **14**, 235–248.
57. B. Hinrichsen, R. E. Dinnebier, and M. Jansen, in *Commission on Powder Diffraction. Hrsg.: Int. Union of Crystallography Newsletter.*, 2005, pp. 12–22.
58. J. L. Flippen, R. D. Gilardi, and IUCr, *Acta Crystallogr. Sect. B Struct. Crystallogr. Cryst. Chem.*, 1975, **31**, 926–928.
59. A. L. Grzesiak and A. J. Matzger, *J. Pharm. Sci.*, 2007, **96**, 2978–2986.
60. T. V. Timofeeva, G. H. Kuhn, V. V. Nesterov, V. N. Nesterov, D. O. Frazier, B. G. Penn, and M. Y. Antipin, *Cryst. Growth Des.*, 2003, **3**, 383–391.
61. F. H. Allen, *Acta Crystallogr. B.*, 2002, **58**, 380–388.
62. A. Tilborg, B. Norberg, and J. Wouters, *Eur. J. Med. Chem.*, 2014.
63. I. Halasz, A. Puškarić, S. a J. Kimber, P. J. Beldon, A. M. Belenguer, F. Adams, V. Honkimäki, R. E. Dinnebier, B. Patel, W. Jones, V. Strukil, and T. Friščić, *Angew. Chem. Int. Ed. Engl.*, 2013, **52**, 11538–41.
64. F. Fischer, D. Lubjuhn, S. Greiser, K. Rademann, and F. Emmerling, *Cryst. Growth Des.*, 2016, **16**, 5843–5851.
65. L. Batzdorf, F. Fischer, M. Wilke, K.-J. Wenzel, and F. Emmerling, *Angew. Chemie Int. Ed.*, 2015, **54**, 1799–1802.
66. D. Gracin, V. Strukil, T. Friščić, I. Halasz, and K. Užarević, *Angew. Chem. Int. Ed. Engl.*, 2014, **53**, 6193–7.

67. K. Užarević, I. Halasz, and T. Friščić, *J. Phys. Chem. Lett.*, 2015, **6**, 4129–4140.

